Influence of pressure cycling on damage evolution in an unfilled EPDM exposed to high-pressure hydrogen

Hiroaki Ono, Azdine Nait- Ali, Ousseynou Kane Diallo, Guillaume Benoit, Sylvie Castagnet

Influence of pressure cycling on damage evolution in an unfilled EPDM exposed to high-pressure hydrogen

Hiroaki Ono, Azdine Nait-Ali, Ousseynou Kane Diallo, Guillaume Benoit, Sylvie Castagnet

Abstract This study aims to reveal the internal damage evolution process in a transparent ethylene propylene diene rubber (EPDM) under high-pressure hydrogen cycles (9 and 15 MPa). Damage accumulation of EPDM was tracked from in-situ pictures during cycling. Several dedicated image processing routines allowed the discrimination of mechanisms (separated cavities, clusters and cracks) and sometimes the qualification of their morphology (size distribution, number, ratio of cavities reappearing at any cycle). Numerous small cavities were observed at any cycle, some of them being clustered under the highest pressure. Only part of them systematically appeared again. Some of these cavities inflated and "absorbed" small cavities around them when clustered. Finally, a few cracks were nucleated from some large cavities and grew, following a "stop and grow" process.

Keywords Cavitation · Cracking · In-situ observation · Photography · Image analysis · Rubber

H. Ono (✉) · A. Nait-Ali · O. Kane Diallo · G. Benoit · S. Castagnet
Département de Physique et Mécanique des Matériaux, Institut Pprime, UPR CNRS/Isae-Ensma/Université de Poitiers 3346, 1 Avenue Clement Ader, BP 40109, 86961 Chasseneuil-Futuroscope Cedex, France
e-mail: ono.hiroaki.340@m.kyushu-u.ac.jp

Present address
H. Ono
Research Center for Hydrogen Industrial Use and Storage (HYDROGENIUS), Kyushu University, Motooka Nishi-ku, Fukuoka 819-0395, Japan

1 Introduction

Rubber materials are generally used for gas sealing. In fuel cell vehicle (FCV) and hydrogen station for fuelling hydrogen gas to FCV, hydrogen gas is stored in high-pressure proof tanks under high-pressure up to 70 and 90 MPa, respectively. And the high-pressure hydrogen gas flows in the pipe lines and fuelling nozzle of FCV and of the station. Fuelling hydrogen from the station to FCV is done by using deferential pressure between FCV and the station. Rubber materials are used as a high-pressure hydrogen gas seal O-ring in these systems. The rubber materials are thus cyclically exposed to high-pressure hydrogen gas.

It has been reported that rubber materials exposed to high-pressure gas, including argon, nitrogen, carbon dioxide and methane, exhibit internal cavitation and cracking (Gent and Tompkins 1969; Stewart 1970; Briscoe and Zakaria 1990; Briscoe et al. 1994; Embury 2004). These mechanisms are caused by the reduction of solubility of dissolved gas accompanying with rapid removal of ambient gas pressure surrounding the rubber. Also in the case of high-pressure hydrogen gas, occurrence of these types of mechanisms has been reported (Jaravel et al. 2011, 2013; Kane-Diallo et al. 2016; Yamabe et al. 2011; Yamabe and Nishimura 2009, 2013; Koga et al. 2011). These types of mechanisms can obviously lead to the fatal fracture of high-pressure hydrogen gas seal O-ring. This kind of damage could be observed only when cyclic exposure test is finished and the O-ring is taken out from the test machine.

Thus, it has been possible to observe the resulting damage, but not the evolution of the damage process. For confidence in the high-pressure hydrogen seal O-ring, understanding how damage evolves is important.

Cavitation inside of rubber materials induced by single and cyclic mechanical loading has deeply been investigated by using not only mechanical tests but also in-situ photography, small angle X-ray scattering and X-ray tomography (Lindsey 1967; Bayraktar et al. 2008; Cristiano et al. 2010; Hocine et al. 2011; Legorju-Jago and Bathias 2002; Zhang et al. 2012, 2013). In general, it has been accepted that the cavitation induced by mechanical loading originates from dilatation of a "precursor" by local hydrostatic pressure.

In the case of cavitation by gas exposure, including pressurization and depressurization process, it is known that a gas dissolved in a "cavity-precursor" of a rubber material during pressurization expands the precursor from the inside during depressurization (Gent and Tompkins 1969; Stewart 1970; Yamabe and Nishimura 2009; Jaravel et al. 2013).

As limiting to only hydrogen gas exposure cases, Yamabe and Nishimura were probably first researchers who investigated the cavitation inside rubber materials induced by high-pressure hydrogen gas pressurization and subsequent depressurization (Yamabe and Nishimura 2009). They defined cavity and cracks induced by high-pressure hydrogen gas exposure as "blister fracture". Subsequently, several researchers have been developing this field.

Jaravel et al. (2011) reported that cavity appearance time after decompression is shortened by elongation, and damage quantities depend on both maximum pressure and depressurization rate in silicone rubber samples under the single high-pressure hydrogen exposure test that was conducted for different maximum pressure (0.1–27 MPa), different depressurization rate (0.2–90 MPa/min) and under elongation. They also attempted to simulate the cavity growth scenario in the above experimental systems using a model with a single initial hole existing at the sample center and took into account internal pressure of cavity, hydrogen content of a cavity, of a rubber matrix and of ambient (Jaravel et al. 2013). Then they indicated that cavity growth inside of rubber can be represented by diffusivity of hydrogen gas and elastic modulus of rubber.

Kane-Diallo et al. (2016) also conducted in-situ observation for transparent EPDM under single high-pressure hydrogen exposure test with different maximum pressure and different depressurization rate, and reported that the number of cavities and the mean cavity diameter is increased by increment and fastening of maximum pressure and of depressurization, respectively.

Above progress of investigations about internal damage of rubber materials by hydrogen exposure considered only single exposure—the test including only one set of pressurization–saturation–depressurization. In the case of real use of high-pressure hydrogen O-ring, as mentioned previously, the O-ring is cyclically exposed to high-pressure hydrogen gas–pressurization–saturation–depressurization-kept at lower pressure and subjected to the subsequent pressurization cycles. Yamabe et al. and Koga et al. attempted the cyclic exposure test for confirmed condition to evaluate cycling effect on internal damage and revealed an incremental number of cracks with cycle progress (Yamabe and Nishimura 2013; Koga et al. 2011). However, it is still unknown how cracks appear and grow through cycling. Thus the investigation of damage evolution under cyclic high-pressure hydrogen gas has not been clarified enough, only the resulting damage has been reported. Hence, in-situ optical tracking of damage morphology during pressurization and depressurization cyclic process is a powerful technique to reveal the damage evolution by cyclic hydrogen exposure.

In this paper, cyclic exposure test up to 9 and 15 MPa were conducted for in-situ observation to chase damage progress in transparent EPDM through the cycling. The test at 9 MPa was employed focusing on cavity growth and the test at 15 MPa was employed for both cavity growth and evolution from cavity to crack.

This paper aims to reveal damage evolution processes under high-pressure hydrogen gas exposure cycling up to 9 and 15 MPa by in-situ photography observation.

2 Experimental

2.1 Sample

For optical damage observation, transparent ethylene–propylene–diene rubber (EPDM) was prepared. The sample was vulcanized under 170 °C for 7 min, from a compound composed of 100 phr (per hundred rubber) of EPDM polymer (ESPREN505, Sumitomo Chemical Co., Ltd.), 0.5 phr of stearic acid and 1.6 phr of

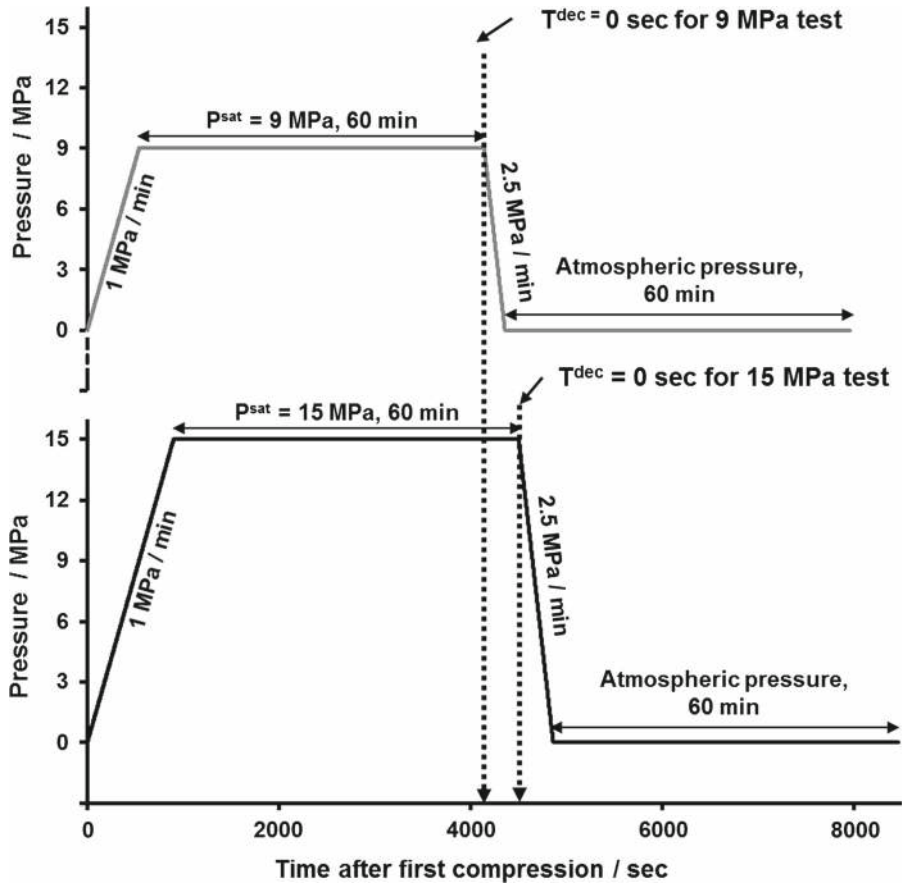

Fig. 1 Schematic illustration of a unit of pressure sequence for 9 and 15 MPa cyclic exposure. The units were repeated 5 and 6 times, respectively, for 9 and 15 MPa test

dicumyl peroxide as a vulcanized agent. The vulcanizate was obtained as a 150 mm × 150 mm × 2 mm sheet from which 20 mm × 20 mm × 2 mm samples were cut out.

2.2 High-pressure hydrogen cycles test

The high-pressure hydrogen cycles tests were conducted in a pressure tight vessel with a ϕ 28 mm × 70 mm thick sapphire glass for optical observation. Figure 1 illustrates the schematics of unit pressure sequences of cyclic hydrogen exposure test for 9 and 15 MPa saturation pressure. The compression rate was 1 MPa/min up to a saturation pressure (P^{sat}) of 9 or 15 MPa. Samples were kept at P^{sat} for 60 min. The decompression rate was 2.5 MPa/min down to atmospheric pressure.

The authors revealed the effect of the decompression rate on damage morphology of transparent EPDM during a single pressure cycle (Kane-Diallo et al. 2016). In that paper, seven decompression rates (0.75–30 MPa/min) were employed. A middle range value of decompression rate (2.5 MPa/min) was selected here to address cycling.

The time between the end of decompression at cycle (n) and the beginning of compression at cycle (n + 1) was 60 min. Such cycle, as shown in Fig. 1, was repeated 5 and 6 times, respectively, for 9 and 15 MPa test. For each cycle, the time elapsed from the beginning of decompression was called T^{dec}.

2.3 Time resolved observation

Figure 2 exhibits the schematic illustrations of the in-situ observation system, an example of a resulted image and the magnified image showing minimum detectable damage. Images were taken with a CCD camera (Sony XCD SX 90) fitted with an Avenir TV Zoom Lens (12.5–75 mm F18). The resolution was 23 μ m/pixel. The image acquisition period was (1) 2 s over the first

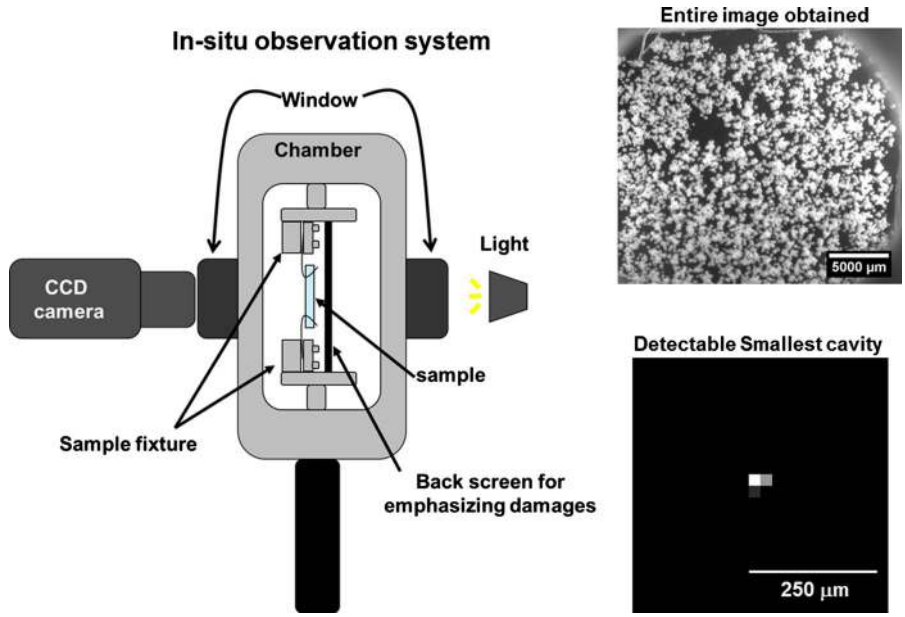

Fig. 2 Schematic illustrations of the in-situ observation system, an example of resulted image and the magnified image showing minimum detectable damage

1200 s after the beginning of compression, (2) then 600 s over the range from 1800 to 4200 s, (3) 2 s between 4202 and 6060 s, (4) and finally 60 s from 6120 to 8460 s.

2.4 Image processing and analysis

Figure 3 shows a schematic illustration of image processing routines. Fiji plug-in of Image J (Available from: http://fiji.sc/Fiji) was used for all image processing and analysis of the high-pressure tests at 15 MPa. Visilog software was used for the low pressure one (9 MPa). The first "(1) Removing background noise" step consisted of subtracting the image of beginning of 1st cycle to each image to remove artefacts such as dust or shaping defects that did not take part to the final damage. Several damage processes affected the samples during cyclic exposure. The aim of the following procedure was to isolate them from each other. Four different treatments were applied depending on the damage process being addressed. They are detailed in Fig. 3, as the processes A–C in the "(2) Image processing routines for each evaluation".

(A) Cavity separation The aim of this routine was to analyze the size of *separated* cavities, so-called by opposition to *clustered* ones. As shown in the left picture, the eye could not separate some contacted cavities from each other. The first step of the routine was thus to remove such clusters (step 1). Then, the remaining recognizable contacted cavities were divided by 2-pixel thick line (step 2). Obtained images were binarized with a 20 threshold on the grey level scale. The average area of cavities (not necessarily spherical) was computed, and the diameter of equivalent spherical cavities could be calculated from it. It was called D in the following.

In the case of low saturation pressure test (9 MPa), no clusters were observed. A segmentation/erosion/spherical reconstruction process, equivalent to steps 2 and 3, were applied to separate cavities from each other and extract their diameter and the location of centroids (Kane-Diallo et al. 2016).

(B) Extraction of the damage area overlapped between cycle n and cycle n + 1 The aim was to be able to quantify persisting damage between two successive cycles. After noise removal, all binarized pictures taken during cycle n were summed up to integrate damage occurring at any time of the cycle (step 1). The same process was applied to the pictures stack of cycle $n+1$. These summed up images were superimposed and colored yellow in areas that appeared to be common damage areas between cycle n and cycle $n+1$ (step 2). The superimposed image was binarized again (yellow area was black and the other color was white) (step 3). This allowed the quantifying of the damage fraction of cycle n survival (meaning observed again) at cycle $n+1$. This common area was called "surviving area" (F^{surv}) in the following.

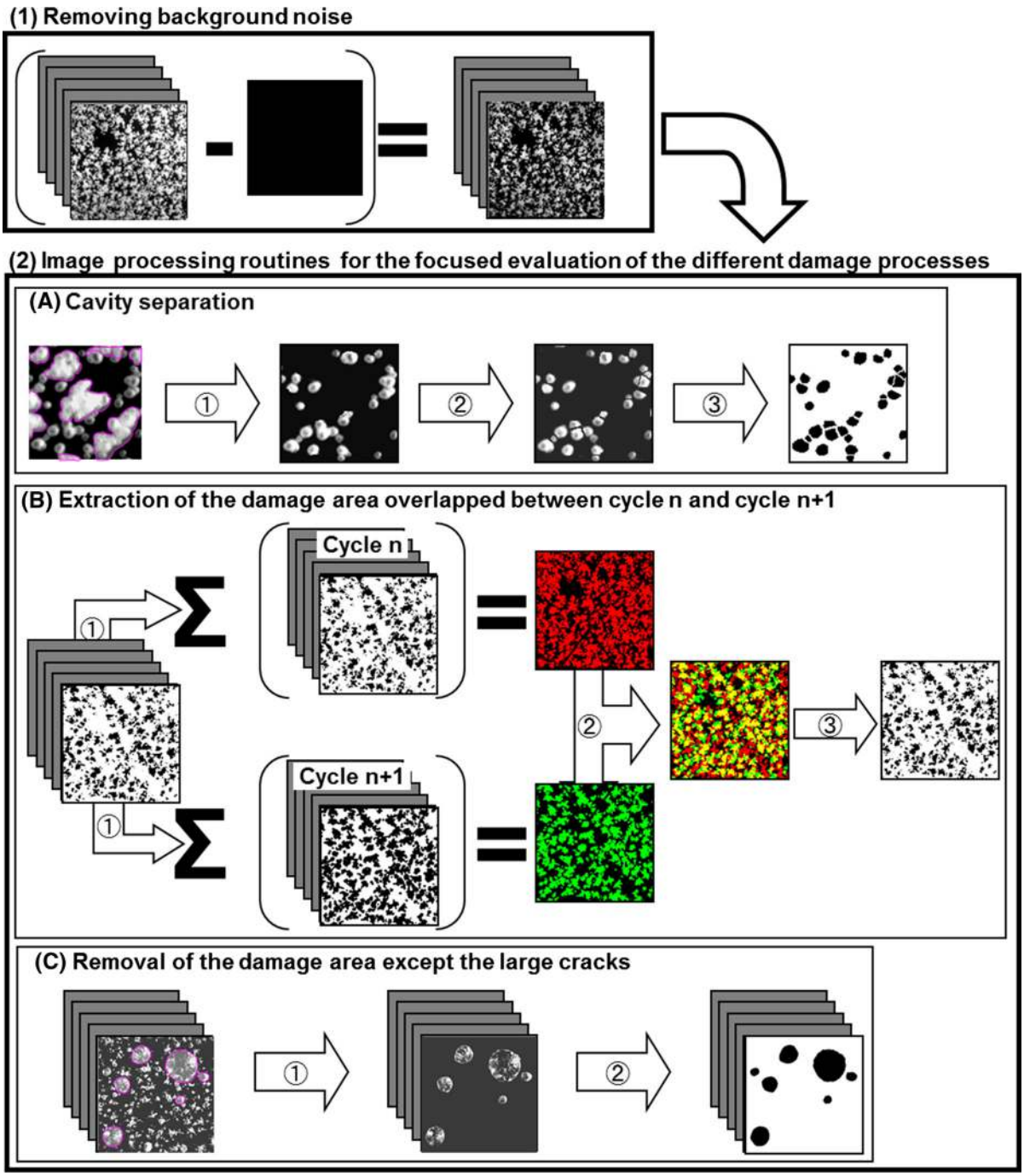

Fig. 3 Overview of the various image processing routines applied for the extraction and the focused analysis of the different damage processes affecting EPDM samples during cyclic exposure to hydrogen at 15 MPa

(C) Removal of the damage area except the large cracks This routine addressed large crack analysis. It was applied to any picture, from any cycle, exhibiting large cracks. Large cracks contour was plotted in order to retain cracks only (step 1). Pictures were binarized again (step 2) in order to compute the equivalent diame-

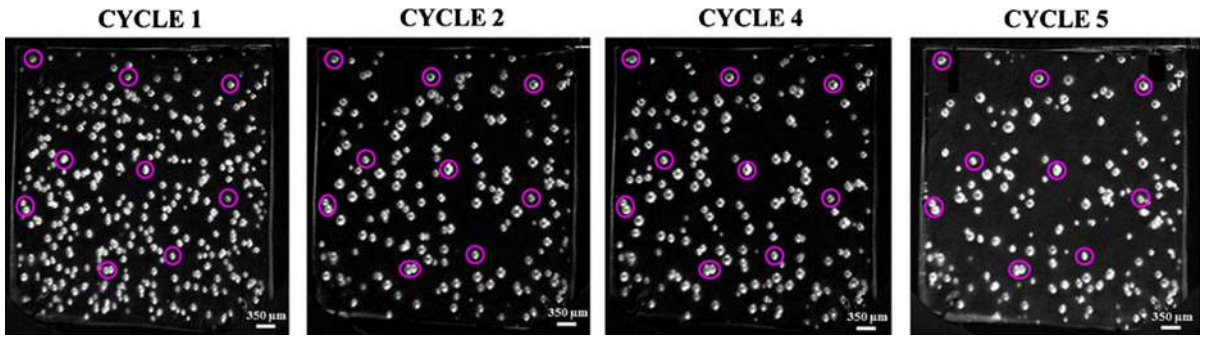

Fig. 4 Evolution of cavity fields observed along cycling up to 9 MPa. The cavities circled with red line means cavities appeared at each cycle defined as "surviving cavities" in this paper

ter of each crack. This was used to appreciate the cracks inflation during one given cycle or between two cycles.

3 Results

Samples were exposed to several cycles of hydrogen pressure up to a maximum pressure (P_{sat}) of 9 or 15 MPa. In the former case, only separated cavities were detected whereas in the latter case, other forms of damage appeared, like clustering or cracking. General features of the damage morphology are depicted for these more or less severe exposure conditions in the first following section. Each damage mode is later considered more in-depth in the next paragraphs.

In this paper, the terms "cavity" and "crack" were both used to depict the damage morphology observed in 9 and 15 MPa tests. Such terms usually refer to the shape of defects (spherical vs. thin and elongated), associated with variable stress concentrations and usually handled by damage mechanics or fracture mechanics. In the present case, terms were particularized to the observed damage morphology. "Cavity" referred to a smaller defect than a "crack". As detailed in the following sections, cavities could disappear, or re-appear and grow, during cycling. Cracks referred to irreversible large defects, growing from coalescent surrounding cavities up to sizes comparable to the sample thickness and sometimes bursting at the surface of the sample.

3.1 Evolution of damage morphology

This first section gives a general description of the observed damage morphology in samples exposed to cycles up to 9 or 15 MPa. Each damage process will be quantified in the following sections. The low-pressure test (9 MPa) is considered first, due to the reduced number of activated damage processes compared to the high-pressure test (15 MPa). Typical damage observed in samples cycled up to 9 MPa is thus illustrated in Fig. 4.

Pictures correspond to the maximum number of cavities for each cycle. Such states were reached after shortening times with cycling. The number of cavities clearly decreased with cycling, meanwhile the average size increased. By carefully considering pictures, it could be detected too that some cavities appeared at each cycle as shown in Fig. 4 whereas some others were not systematically observed. The former ones are called "surviving cavities" in the following.

The thickness of the chamber door and the small size of the window clearly limited the spatial resolution of observations and, subsequently, the ability to track cavity expansion in the thickness direction. Some attempts showed that cavities grow in the thickness direction too but 2D pictures on the edge of the sample were not good enough for detailed analysis.

Under more severe conditions, i.e., up to a higher saturation pressure of 15 MPa, the damage morphology was more complex. As attested by Fig. 5, clusters and large cracks co-existed with separated cavities.

During the first decompression (Fig. 5a–c), separated cavities began to appear (see cycle 1 in Fig. 5a). Then, the number of cavities, as well as their size, increased with time. Unlike in the 9 MPa test, some cavities formed clusters, as shown in Fig. 5b. After maximum damage, a deflation process started during the last part of cycle 1. When the sample was com-

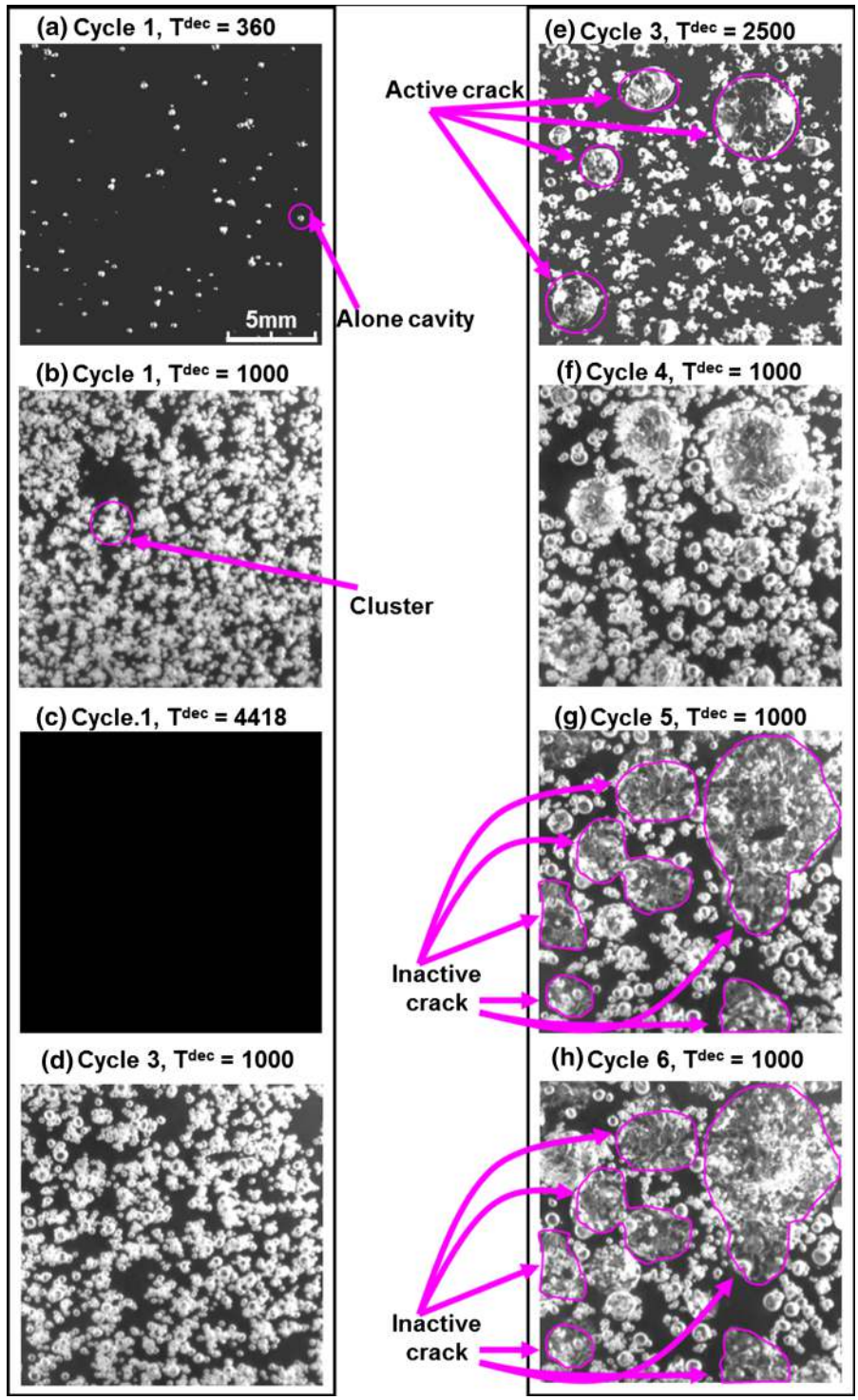

Fig. 5 Damage morphology observed in samples cycled up to 15 MPa in; **a** cycle 1 at 360 s after beginning of decompression ($T^{dec} = 360$), **b** cycle 1 at $T^{dec} = 1000$, **c** cycle 1 at $T^{dec} = 4418$, **d** cycle 3 at $T^{dec} = 1000$, **e** cycle 3 at $T^{dec} = 2500$, **f** cycle 4 at $T^{dec} = 1000$, **g** cycle 5 at $T^{dec} = 1000$ and **h** cycle 6 at $T^{dec} = 1000$

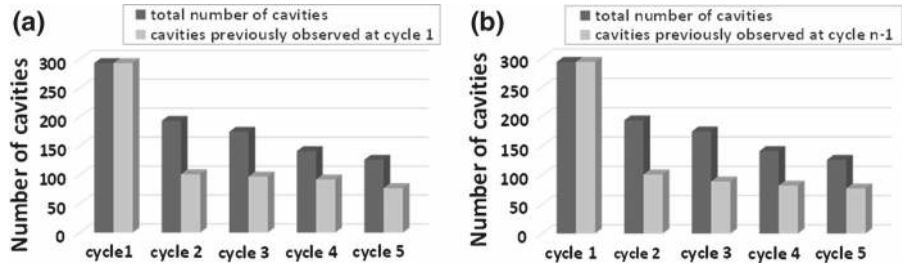

Fig. 6 Total number of cavities and number of "surviving" cavities, i.e., previously observed **a** at the first cycle and **b** at the previous cycle (cycling up to 9 MPa, decompression at 2.5 MPa/min)

pressed again at the beginning of cycle 2, both separated cavities and clusters deflated with the pressure increase, and finally disappeared, as shown in Fig. 5c.

The same scenario was repeated at cycle 2. In cycle 3, cavities and clusters were observed again at 1000 after the beginning of the third decompression same as cycle 2, as shown in Fig. 5d. However, from 1129 s, some of the cavities restarted to inflate and turned to cracks, as shown in Fig. 5e. Such cracks were called "active" as long as their size evolved, either with time during a given cycle, or from one cycle to another.

During the compression process, clusters and active cracks deflated with the pressure increase and finally disappeared, like in cycles 1 or 2. At cycle 4, cavities and active cracks all appeared at the same places as at cycle 3 (Fig. 5f). Active cracks continued growing. Some of the remaining cavities began to inflate again and became active cracks too. The active cracks which had propagated between cycles 3 and 4 turned to "inactive" cracks at cycle 5, meaning that their size did not evolve any more until the end of cycle 6 (as shown in Fig. 5g, h).

3.1.1 Process 1: separated cavities

This elementary damage mechanism was observed in both samples cycled under 9 and 15 MPa. The case of tests at 9 MPa will be considered first; in such moderate decompression conditions, all cavities can be considered as "separated cavities" following the above defined terminology. Pictures were processed to obtain the number and size of cavities. Figure 6 displays the maximal number of cavities for each cycle (left dark grey columns). It significantly decreased, especially between cycles 1 and 2, and was almost divided by two after 5 cycles. The right columns (light grey columns) correspond to the number of "surviving" separated cavities, i.e., the number of separated cavities already observed at cycle 1 in Fig. 6a and at the previous cycle in Fig. 6b. The graphs show that the view of a cumulative damage (i.e. a progressive growth of the same population of cavities cycle after cycle) is erroneous. Indeed, separated cavities observed at cycle 1 did not systematically appear again during the following cycles. However, their relative number increased with cycling. A large majority of the separated cavities observed at cycles 4 and 5 were already visible at the previous cycle and more generally from the first cycle. A more detailed analysis showed that surviving cavities previously reached a diameter larger than 190 μm.

Figure 7a represents the size distribution of separated cavities for each cycle, when the number of cavities was the largest. Histograms of the major population are shifted towards high values and narrowed with cycling, supporting homogenization of cavity size with cycling. A minor population of small cavities also appeared at cycles 2 and 3 but later disappeared. Figure 7b shows the evolution of the average diameter of Fig. 7a through cycling. The average diameter increased with cycle until cycle 3 and became constant in remaining subsequent cycles.

Let us consider now more severe decompression conditions. Images taken from samples cycled up to 15 MPa were first processed as detailed in Fig. 3 [process (A)] to isolate separated cavities. The area A of each separated cavity was measured and used to calculate the diameter D of an equivalent spherical cavity with identical area, as shown in Eq. (1).

$$\mathrm{D} = 2\left(\frac{A}{\pi}\right)^{\frac{1}{2}} \tag{1}$$

Figure 8a shows the separated cavity diameter distribution over 0.1 mm wide ranges for cycles 1–6 at $\mathrm{T}^{\mathrm{dec}} = 1000$ s for all cycles. This time corresponded to the maximum value of damage occupied area.

As shown in Fig. 8a, the curves show approximately the normal distribution for cycles 1 and 2, with an aver-

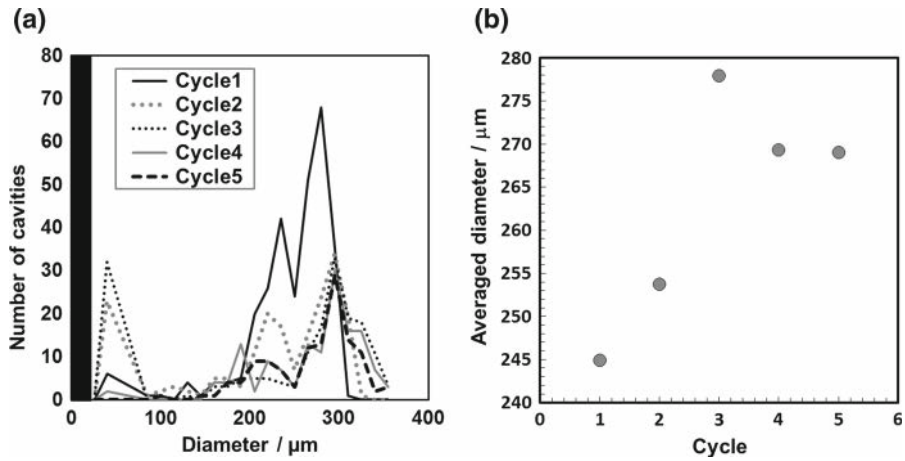

Fig. 7 **a** Evolution of the size distribution of cavities with cycling at 9 MPa and 2.5 MPa/min (at the maximum size of cavities for each cycle). The dark zone in the plot means the region below the lower size limit of camera resolution. **b** Averaged cavity size evolution through the cycling

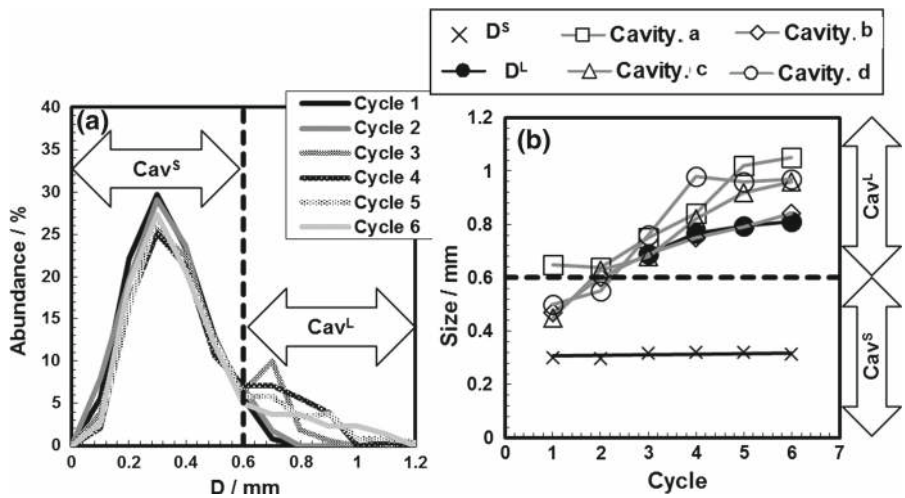

Fig. 8 **a** Distribution of separated cavity diameter at $T^{dec} = 1000$ s for each of the six cycles and **b** equivalent diameter of several populations of cavities (D^S, D^L) and diameter of some separated cavities a, b, c, d (location visible in Fig. 9)

age value close to the mode value of 0.3 mm. This damage pattern is consistent with the major population observed in Fig. 7a in samples tested up to 9 MPa.

From cycles 3 to 6, curves clearly did not obey normal distribution any more. Indeed, the curves showed approximately the same shape as cycles 1 and 2 in the range from 0.1 to 0.6 mm but a shoulder appeared above 0.6 mm. Although the mode value was unchanged (0.30 mm), the average values increased from cycles 3 to 6 (respectively 0.35, 0.38, 0.39 and 0.37 mm).

Judging from size distribution of separated cavities in a 15 MPa test, two different populations could be distinguished. The small separated cavities (Cav^S) corresponded to the main peak in size distribution as shown in Fig 8a. The large separated cavities (Cav^L) corresponded to the shoulder of the main peak towards high diameter values as shown in Fig 8a, i.e. above 0.6 mm.

The average equivalent diameter of each population (respectively D^S and D^L) was calculated following Eq. (1) and plotted in Fig. 6b. D^S was almost the same for all cycles (0.30 mm). D^L slightly increased between cycles 3 and 5 and was almost constant at approximately 0.8 mm between cycles 5 and 6.

To highlight the origin of large cavities observed from cycle 3, a few single separated cavities (called a–d) were tracked along cycling. Their location is depicted in Fig. 9 in pictures taken at $T^{dec} = 1000$ s. Figure 8b shows an increase in their diameter. Cavities a, b, c and d appeared at the same place thorough all cycles, but it is important to notice that during the first cycles, they pertained to collections of very close small cavities whereas they later appeared as separated cavities in the last cycles.

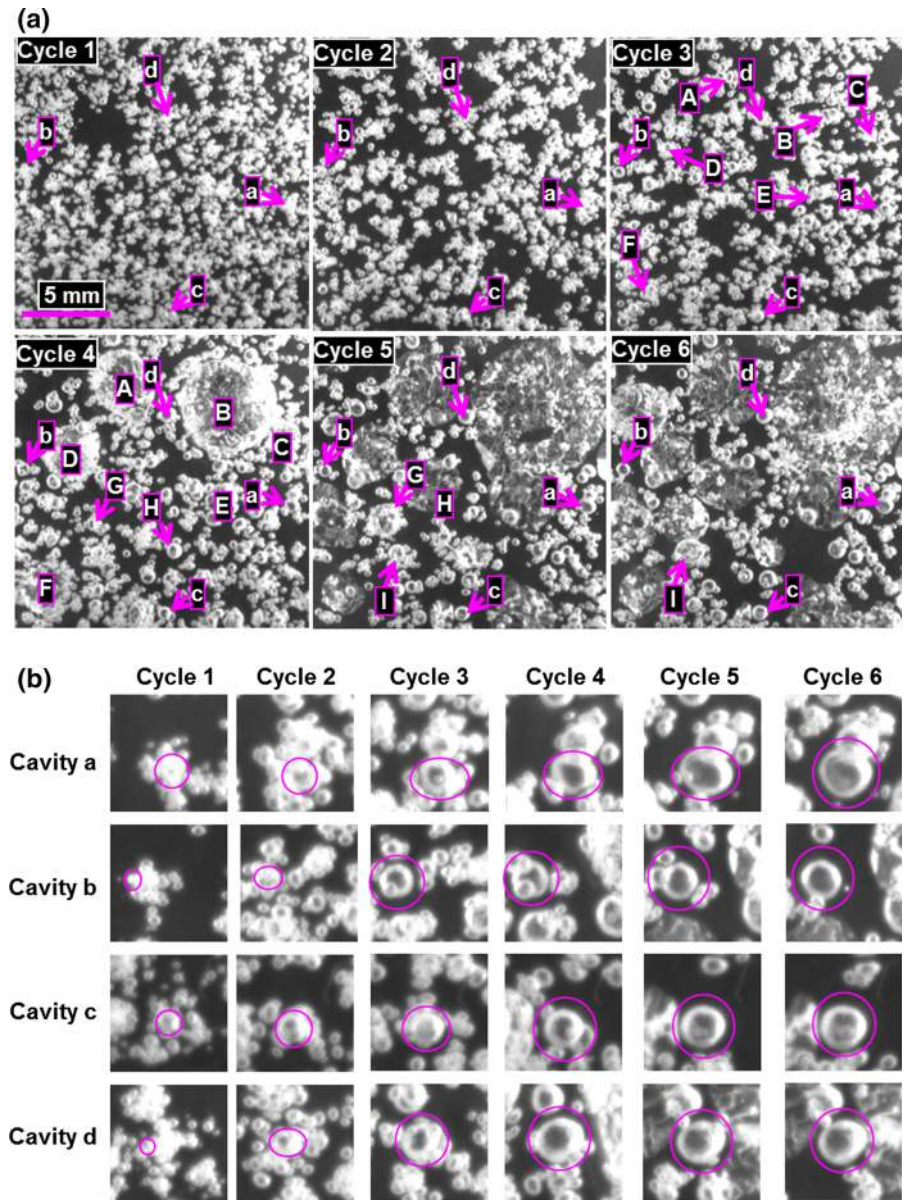

Fig. 9 **a** Views of damage at $T^{dec} = 1000$ s at each cycle, including some separated cavities (a–d) and cracks (A–I) quantitatively analyzed in the work. **b** The magnified images focusing on cavity a–d

The effect of "surviving" cavities was addressed too in high-pressure conditions, in the same way as for 9 MPa tests. Figure 10 shows the damage fraction of cycle n survived in cycle n + 1 (F^{surv}), as calculated by Eq. (2).

$$F^{surv} = \frac{A^n \cap A^{n+1}}{A^n} \tag{2}$$

where A^n is the area occupied by damage in cycle n and A^{n+1} is the area occupied by damage in cycle n + 1. It must be highlighted that both small and large separated cavities were taken into account in such analysis.

Images were summed up to take into account all damage history in cycle n and cycle n + 1, according to process (B) illustrated in Fig. 3. As shown in Fig. 10, F^{surv} significantly increased; it was almost twice as large after 6 cycles as at the first cycle: for cycles 6 and 1, F^{surv} was, respectively, 0.81 and 0.49. This result was fully consistent with that obtained at lower pressure (Fig. 6b).

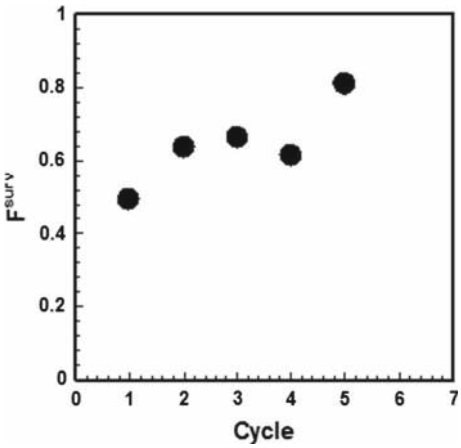

Fig. 10 The damage fraction of cycle n surviving in cycle n + 1 (F^{surv})

3.1.2 Process 2: cracking

This damage mechanism was only observed at the higher pressure (15 MPa). To track the evolution of the few actual cracks, images were processed following the routine C illustrated in Fig. 3. The diameter of equivalent circular cracks was then calculated in the same way as previously done for separated cavities, from Eq. (1).

Through cycles 3–4, six cracks were nucleated, indexed as crack A to F in Fig. 9. Through cycles 4–5, and then cycles 5–6, respectively, two and one more new cracks were also observed, which were, respectively, indexed as crack G, H and I in Fig. 9.

As shown in Fig. 9, damage morphology was still composed of cavities at $T^{dec} = 1000$ s in cycle 3. Cracking begun from part of these cavities being the "crack precursor" of crack A–F indexed in Fig. 9.

Figure 11 shows life time of crack A; (a) time evolution of the equivalent diameter [calculated from Eq. (1)] of crack A for cycles 1–4 as an example of crack A–I, (b) magnified images of crack A corresponding to each selected time written in the Fig. 11a with arrow. The images of cycles 5 and 6 were added to show "inactive" states. As shown in Fig. 11, crack A had not been "crack" yet, just a cavity in cycles 1 and 2. In other cracks (B–I), the cavities began to appear at cycles 1 or 2. A first growth step was observed at the beginning of cycle 3, followed by a "plateau" which means a tentative stop of the cavity growth as shown in Fig. 11a, b as Cycle 3, $T^{dec} = 360$ and Cycle 3, $T^{dec} = 2417$. The equivalent diameter of cavity during plateau was similar at cycle 3: 0.82, 0.69, 0.77, 0.71, 0.71 and 0.60 mm, respectively, for cracks A to F. Theses cavities are assignable to Cav^L judging from their size, and their abundance is equivalent to at least 10% of Cav^L in the size range of 0.6–0.9 mm. Thus, remaining 90% of Cav^L was still cavity till the end of cycle 3. This constant stage for cracks A to F lasted until $T^{dec} = 2417$, 1129, 2597, 1129, 1129 and 2837 s, respectively. Following that, the cavity growth restarted until the beginning of compression of the next cycle and becoming the large crack as shown in the images of Cycle 3, $T^{dec} = 2472$ and Cycle 3, $T^{dec} = 3917$ in Fig. 11b.

During the decompression process of the following cycle (cycle 4), it was very interesting to note that the crack quickly re-opened to the previous maximum size measured at cycle 3, as shown in image Cycle 4, $T^{dec} = 360$ in Fig. 11. Then, the following propagation stage was slower, until reaching a maximum equivalent size to that of cycle 3, except crack B, C and E.

Figure 12 exhibits magnified images focusing on crack B, C and E at $T^{dec} = 754$, 1194 and 1756 in cycle 4. As shown in Fig. 12, crack B, C and E coalesced. This coalesced crack also continued to grow until the maximum size.

After reaching maximum size, the equivalent diameter quickly decreased. This corresponds to the burst of the crack; as shown in images of Cycle 4, $T^{dec} = 1400$ and $T^{dec} = 1402$ in Fig. 11, the change of the brightness of the crack can be found. This originates from the shrink of the crack. Taking into account that the shrink was completed at least within 2 s, it could be thought that the crack bursted with the quick release of hydrogen gas from the inside of the crack to the sample surface.

Figure 13 shows the time evolution of the equivalent diameter [calculated from Eq. (1)] of some of these cracks: (1) crack A for cycles 3–4 as an example of crack A–F (top), (2) Crack G for cycles 4–5 (middle), and (3) crack I for cycles 5–6 (bottom). As shown in Fig. 13, the same process as crack A to F through cycles 3–4 (stop and grow in a cycle and quick re-opening and burst in subsequent cycle) was observed for propagation of crack G, H and crack I, respectively, through cycles 4–5 and through cycles 5–6, as illustrated in the middle and bottom of Fig. 13, respectively.

As long as this step propagation process occurred, the crack was called "active" crack. Some of them finally burst at the surface of the sample. No more

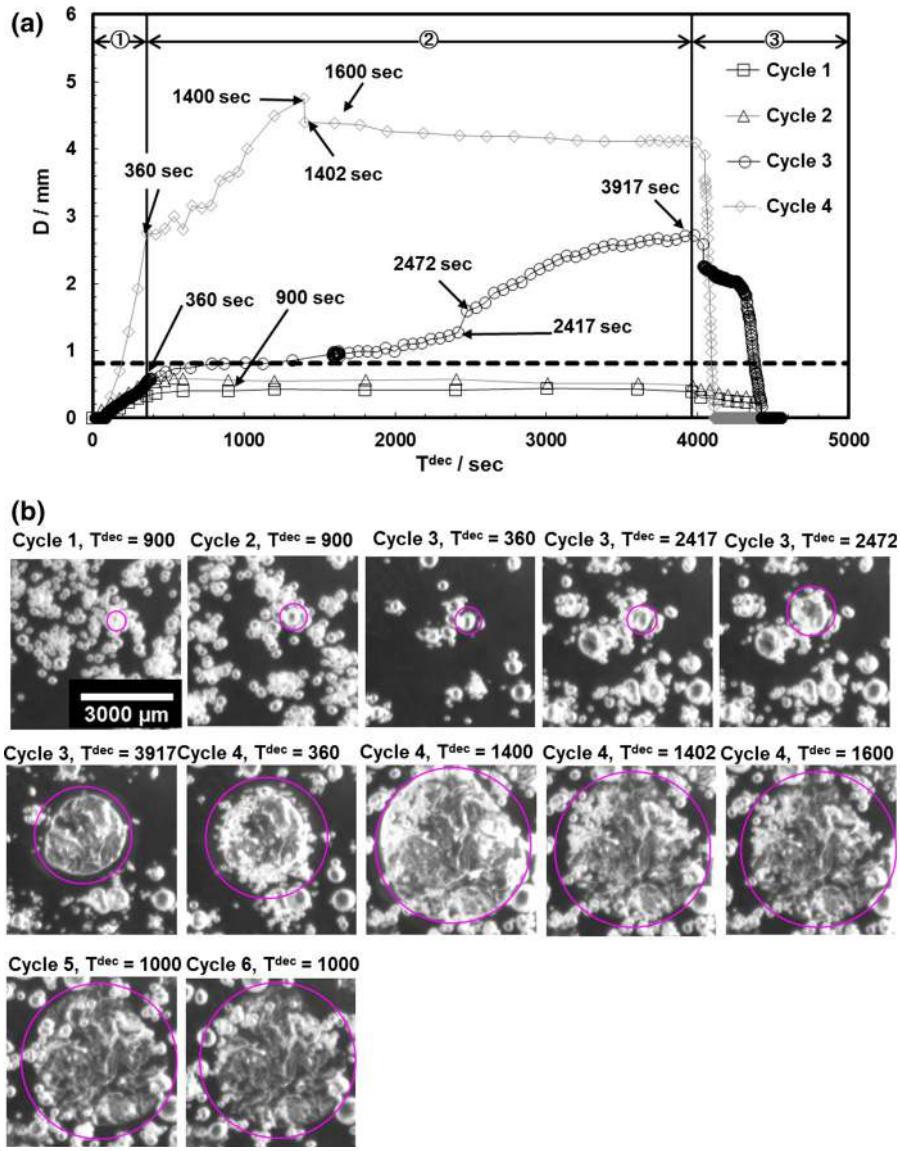

Fig. 11 Tracking of life time of crack A as an example of crack A–I; **a** time evolution of the equivalent diameter [calculated from Eq. (1)] of crack A for cycles 1–4, **b** magnified images of crack A corresponding to each selected time written in the Fig. 11a with arrow. The images of cycles 5 and 6 was added to show "inactive" state

hydrogen could be stored inside the crack during following cycles and the size did not change any more (as shown in image g and h of Fig. 3 and Cycle 4, $T^{dec} = 1600$ in Fig. 11). The crack was then called "inactive".

4 Discussion

The two pressure conditions explored (9 and 15 MPa), respectively, focus on the evolution of separated cavities and on the transition from cavitation to cracking. Judging from above results, a damage evolution scenario until large cracking could be proposed. It is illustrated in Fig. 14. Each process in Fig. 14 is described below:

4.1 Damage appeared as clusters and separated small cavity: Cav^S in first cycles

Cycles 1 and 2 of the 15 MPa test showed only cluster of cavities and small separated cavities. The clustering effect could be brought closer to the onset of satellite cavities growing around primary ones, reported by Gent and Tompkins in CO_2, Ar and N_2 in several kinds

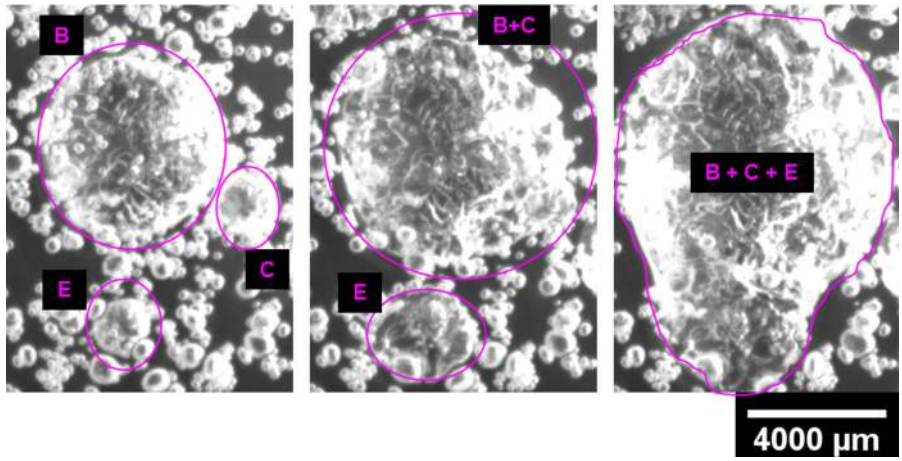

Fig. 12 Magnified images focusing on crack B, C and E at T^{dec} = 754, 1194 and 1756 in cycle 4

of rubber samples (Gent and Tompkins 1969). Jaravel et al. also reported this damage process in hydrogen decompression tests for silicone rubber (Jaravel et al. 2011). At lower pressure (9 MPa), this clustering effect was not observed.

Small separated cavities exhibited smaller average size at 9 MPa (diameter below 0.4 mm), compared to 15 MPa (diameter below 0.6 mm). Kane-Diallo et al. (2016) reported that the number and the average diameter of cavity increase with the decompression rate increase for 9 MPa hydrogen decompression test. In the case of the test at 15 MPa test and the test at 9 MPa for this paper, the saturation pressure was different but the decompression rate was same at 2.5 MPa/min. Hence, it was indicated that the cavity size difference between the 15 MPa test and the 9 MPa test depends on the difference of dissolved hydrogen content and differential pressure between inside of the cavity and the ambience of the sample originated from saturation pressure.

4.2 Parts of the small cavities (Cav^S) disappear as the cycle progresses

According to Fig. 8a, the abundance of separated large cavities (Cav^L) increased to the detriment of small separated ones (Cav^S). According to Fig. 10, the ratio of "surviving" damage F^{surv} increased. When considering cycles 1 and 2, for which separated cavities are "small" ones Cav^S, it means that approximately 50% of Cav^S of cycle 1 disappeared in cycle 2. In the same way, test at 9 MPa showed a global trend to nucleate less numerous but larger separated cavities with cycling. At this pressure too, the ratio of surviving cavities increased, suggesting the growth of a non-negligible fraction of small cavities, but the disappearing of another part of them.

4.3 Parts of Cav^S survive and change to Cav^L with cycling

Part of the population of small cavities Cav^S dead with cycling, as mentioned above, means the residual Cav^S survive through the cycling in the test at 15 MPa. This tendency, i.e., the disappearing of smaller cavities and appearing of larger cavities through the cycling, was the same in the test at 9 MPa, which was also discussed above. According to Fig. 8b, cavity a to d, which were picked up as surviving separated cavities, had a diameter below 0.6 mm (i.e. within Cav^S range) at cycles 1 and 2, and later exceeded 0.6 mm (i.e. within Cav^L range) after cycle 3. These results indicated that some small cavities inflated as a result of a surviving and growing process with cycling.

Moreover, this growing process sometimes interfered with cluster evolution. As observed for instance in cavities c and d in Fig. 9, the collection of small cavities surrounding these cavities at the first cycles disappeared step by step with cycling. Small surrounding cavities seemed to be trapped by the most growing one.

4.4 Parts of the Cav^L evolve to an active crack

According to Fig. 8a, the size distribution and the average equivalent diameter of large separated cav-

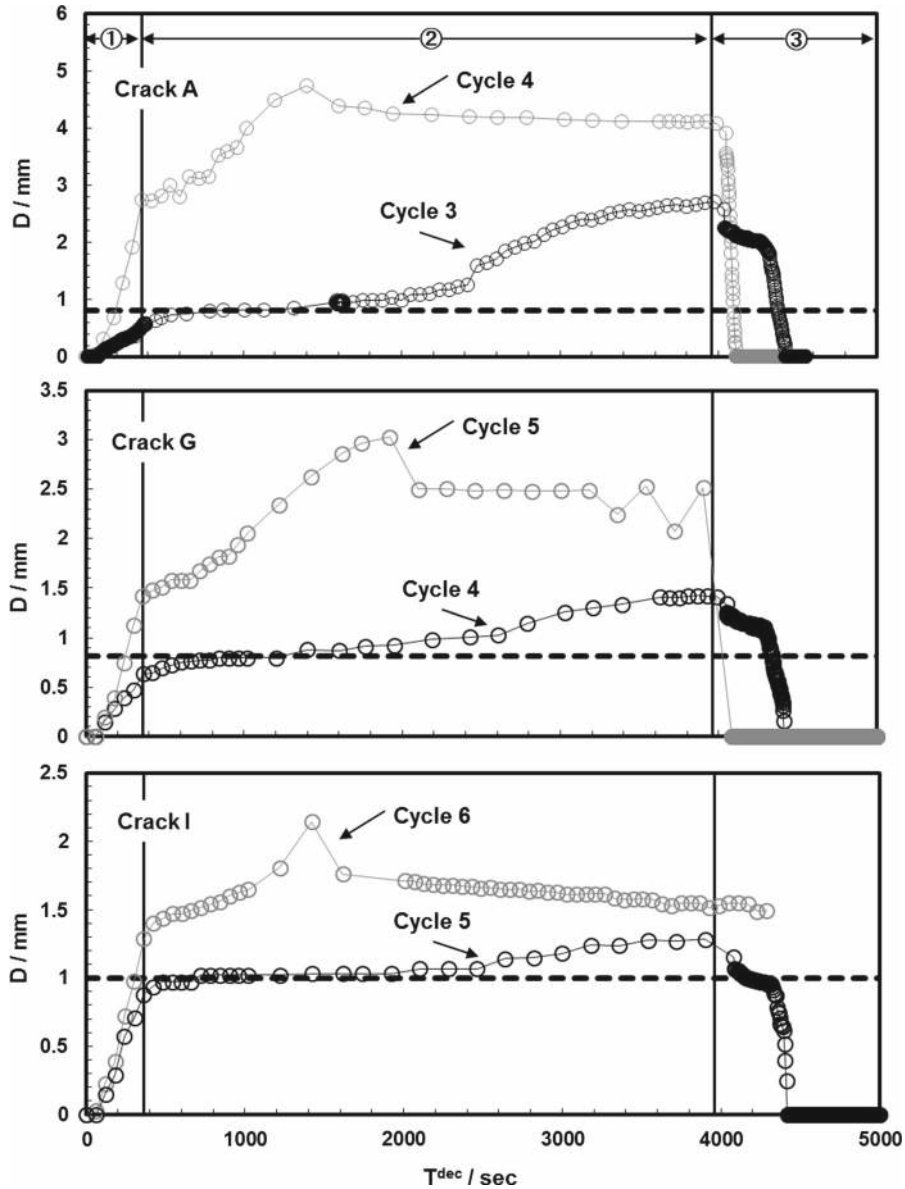

Fig. 13 Comparison of the time evolution of the equivalent crack diameter of cracks during successive cycles: Crack A at cycles 3 and 4 (top), Crack G observed at cycle 4 and 5 (middle) and Crack I observed at cycles 5 and 6 (bottom). T^{dec} is the decompression time of each cycle; period ① refers to the decompression stage, ② to the atmospheric pressure stage and ③ to the following compression stage. Cycle 6 have no decompression process because cycle 6 was the last cycle for the test

ities increased with cycling. Focusing on the crack-precursor cavity size, they were almost the same at 0.7 mm. According to the "*Process 2: cracking*" section, the cavity diameter just before the onset of cracks A to F was approximately 0.7 mm, which was within the Cav^L diameter range. One could wonder whether this size of 0.7 mm could be regarded as a size criterion of the crack-precursor cavity, considering that no cracks were observed in the 9 MPa test in which no cavities exceeded 0.7 mm. However, according to Fig. 8a, some cavities with diameters larger than 0.7 mm still existed until cycle 6 in the 15 MPa test. Finally, this seemingly "critical" size of 0.7 mm could not be regarded as fracture criterion. It could be argued that not only the crack-precursor cavity causes this, but also the surrounding stress field of that was part of the conditions for crack initiation.

The cracks always exhibited a larger diameter than the sample thickness, namely, the cracks always propagated along in-plane direction. Lindsey reported that the tearing direction is perpendicular to the principal tensile stress direction judged by the result of triaxial

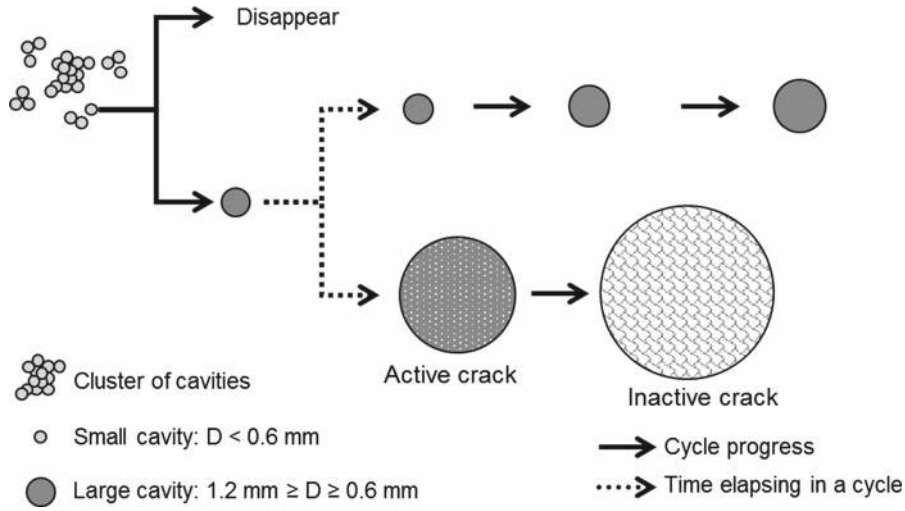

Fig. 14 Schematic illustration of damage shape evolution through the hydrogen exposure cycle

tensile test by using the poker-chip test for negative hydrostatic pressure effect on the damage propagation (Lindsey 1967). It was thus assumed that the crack propagation also activated the principal stress direction perpendicular to the in-plane due to the change of the surrounding stress field, which possibly originates from the size change of cavities except the crack-precursor. The norm of this "mode I"-like process also corresponds to the shortest diffusion path from the core of the sample to the nearest free surface. As the damage mechanism is known to arise from diffuso-mechanical coupling, it could also affect the crack propagation direction.

4.5 The active cracks finally burst and turn to inactive cracks

This process was evidenced from Figs. 9, 11 and 13. It was assumed that the burst–rapid deflation–of the crack was caused by the rapid hydrogen gas desorption from inside of the active crack to the outside of the rubber matrix through the pass due to the crack reaching the surface of the rubber.

5 Conclusion

This study focused on the evolution of damage during successive pressure release in a rubber exposed to high-pressure hydrogen cycles, with a special interest in the transition from cavitation to cracking. The work was based on in-situ direct optical observations of transparent EPDM samples exposed to 9 or 15 MPa of hydrogen pressure.

Several image processing routines were applied to separately analyse cavities and large crack. Clusters evolution was also considered. These different observations can be summarized as follows. Damages appeared as separated cavities (categorized as "small cavities") and also as clusters for the highest exposure pressure. The average size of these cavities increased with the exposure pressure. Part of these small cavities disappeared during the next cycle but the others still survived and expanded to become relatively large cavities. Regardless, there was always a non-negligible ratio of small cavities at any cycle. Large cavities inflated with cycling and reached a "plateau". A few of these large cavities suddenly restarted to grow and suddenly nucleated "active crack" at one cycle. At the next cycle, the active cracks instantaneously re-opened up to the largest size reached during the previous cycle, propagated slower than decompression stage until reaching a maximum equivalent diameter and then suddenly burst. After burst at the surface of the sample, the driving force of the trapped gas vanished, due to the direct connection to the free surface. Cracks did not propagate anymore and turned to "inactive cracks".

A key observation from this work was that damage evolution cannot be viewed as a cumulative process of cavities which systematically re-appear at any cycle and finally coalesce. More complicated coupled diffuso-mechanical processes seem to govern damage evolution at the local scale.

Acknowledgements Authors are grateful to Pr. S. Nishimura from Kyushu University (Japan) for kindly providing the material of this study. This work was partially Funded by the French Government program "Investissements d'Avenir" (LABEX INTERACTIFS, reference ANR-11-LABX-0017-01).

References

Bayraktar E, Isac N, Bessri K, Bathias C (2008) Damage mechanisms in natural (NR) and synthetic rubber (SBR): nucleation, growth and instability of the cavitation. Fatigue Fract Eng Mater Struct 31(2):184–196

Briscoe BJ, Zakaria S (1990) Gas-induced damage in elastomeric composites. J Mater Sci 25(6):3017–3023

Briscoe BJ, Savvas T, Kelly CT (1994) "Explosive decompression failure" of rubbers: a review of the origins of pneumatic stress induced rupture in elastomers. Rubber Chem Technol 67(3):384–416

Cristiano A, Marcellan A, Long R, Hui CY, Stolk J, Creton C (2010) An experimental investigation of fracture by cavitation of model elastomeric networks. J Polym Sci Part B Polym Phys 48(13):1409–1422

Embury P (2004) High-pressure gas testing of elastomer seals and a practical approach to designing for explosive decompression service. Seal Technol 2004(6):6–11

Gent AN, Tompkins DA (1969) Nucleation and growth of gas bubbles in elastomers. J Appl Phys 40(6):2520–2525

Hocine NA, Hamdi A, Abdelaziz MN, Heuillet P, Zaïri F (2011) Experimental and finite element investigation of void nucleation in rubber-like materials. Int J Solids Struct 48(9):1248–1254

Jaravel J, Castagnet S, Grandidier JC, Benoît G (2011) On key parameters influencing cavitation damage upon fast decompression in a hydrogen saturated elastomer. Polym Test 30(8):811–818

Jaravel J, Castagnet S, Grandidier JC, Gueguen M (2013) Experimental real-time tracking and diffusion/mechanics numerical simulation of cavitation in gas-saturated elastomers. Int J Solids Struct 50(9):1314–1324

Kane-Diallo O, Castagnet S, Nait-Ali A, Benoit G, Grandidier JC (2016) Time-resolved statistics of cavity fields nucleated in a gas-exposed rubber under variable decompression conditions—support to a relevant modeling framework. Polym Test 51:122–130

Koga A, Uchida K, Yamabe J, Nishimura S (2011) Evaluation on high-pressure hydrogen decompression failure of rubber O-ring using design of experiments. Int J Automot Eng 2(4):123–129

Legorju-Jago K, Bathias C (2002) Fatigue initiation and propagation in natural and synthetic rubbers. Int J Fatigue 24(2):85–92

Lindsey GH (1967) Triaxial fracture studies. J Appl Phys 38(12):4843–4852

Stewart CW (1970) Nucleation and growth of bubbles in elastomers. J Polym Sci Part B Polym Phys 8(6):937–955

Yamabe J, Nishimura S (2009) Influence of fillers on hydrogen penetration properties and blister fracture of rubber composites for O-ring exposed to high-pressure hydrogen gas. Int J Hydrog Energy 34(4):1977–1989

Yamabe J, Nishimura S (2013) Failure behavior of rubber O-ring under cyclic exposure to high-pressure hydrogen gas. Eng Fail Anal 35:193–205

Yamabe J, Fujiwara H, Nishimura S (2011) Fracture analysis of rubber sealing material for high pressure hydrogen vessel. J Environ Eng 6(1):53–68

Zhang H, Scholz AK, De Crevoisier J et al (2012) Nanocavitation in carbon black filled styrene–butadiene rubber under tension detected by real time small angle x-ray scattering. Macromolecules 45(3):1529–1543

Zhang H, Scholz AK, Vion-Loisel F et al (2013) Opening and closing of nanocavities under cyclic loading in a soft nanocomposite probed by real-time small-angle x-ray scattering. Macromolecules 46(3):900–913